Inorganic Chemistry

Article

pubs.acs.org/IC

Tuning Interchain Interactions in Two-Dimensional Networks of Mn^{III} Schiff-Base Complexes and Dicarboxylic Acids by Varying the Linker

Yoshitaka Aono,[†] Hiroki Yoshida,[†] Keiichi Katoh,[†,‡] Brian K. Breedlove,[†,‡] Koichi Kagesawa,*[,†,‡] and Masahiro Yamashita*[,†,‡]

[†]Department of Chemistry, Graduate School of Science, Tohoku University, 6-3 Aoba, Aramaki, Aoba, Sendai, Miyagi, Japan 980-8578

[‡]Core Research for Evolutional Science and Technology (CREST), Japan Science and Technology (JST), 4-1-8 Kawaguchi, Saitama, Japan 332-0012

Supporting Information

ABSTRACT: Two-dimensional (2D) coordination polymers consisting of Mn^{III} Schiff-base complexes and dicarboxylic acids, $[\{Mn(salen)\}_4(L1)](PF_6)_2\cdot(CH_3OH)_2$ (**C4**; H_2L1 = adipid acid) and $[\{Mn(salen)\}_4(L2)](PF_6)_2\cdot(CH_3OH)_4$ (**C4′**; H_2L2 = *E*,*E*-1,3-butadiene-1,4-dicarboxylic acid) ($salen^{2-}$ = *N*,*N*′-(ethylene)bis(salicylideneiminato), were synthesized by using a one-pot reaction and characterized by using single-crystal X-ray crystallographic analysis. One-dimensional (1D) chains composed of Mn(salen) dimers, $[Mn_2]$, bridged by carboxylato ligands ($-[Mn_2]-OCO-[Mn_2]-$), were linked by dicarboxylato ligands with *n*-butyl ($-C_4H_8-$) (**C4**) and butadienyl aliphatic groups ($-C_4H_4-$) (**C4′**). From static magnetic measurements on both **C4** and **C4′**, there were ferromagnetic interactions between the Mn^{III} ions through the phenoxo oxygen atoms of the $salen^{2-}$, and antiferromagnetic interactions between the Mn^{III} ions through carboxylato ligands ($-OCO-$). As a result, weak ferromagnetism occurred because of the zigzag-shaped chain structure of **C4** and **C4′**, and magnetic anisotropy for Mn(salen). In the magnetization curves for **C4′**, weak interchain interactions (J_{linker}) occurred through the π-conjugated butadienyl linkers in **C4′**, which **C4** did not have. In other words, changing from saturated to unsaturated aliphatic groups in the dicarboxylic acid linkers resulted in weak interactions between 1D-magnetic chain moieties. Therefore, in the case of only **C4′**, antiferromagnetic phase transition appeared at 2.3 K. Both coordination polymers exhibited slow relaxation of the magnetizations, which originated from SCM moieties, because **C4** and **C4′** showed magnetic correlations. It is noteworthy that alternating current (ac) susceptibilities for **C4′** are frequency-dependent around the Néel temperature. From analysis of the ac susceptibilities for **C4**, α (dispersion coefficient of the relaxation of magnetization) varied linearly with $1/T$. This signifies that **C4** behaved as an SCM with a single relaxation process. On the other hand, in α versus $1/T$ plots for **C4′**, an inflection point was observed at the Néel temperature, indicating that $J_{linkers}$ had an effect on the distribution of the relaxation times. Moreover, the inflection point for **C4′** disappeared when a dc magnetic field was applied. This is the first report showing a direct correlation between an antiferromagnetic phase transition and slow magnetic relaxation.

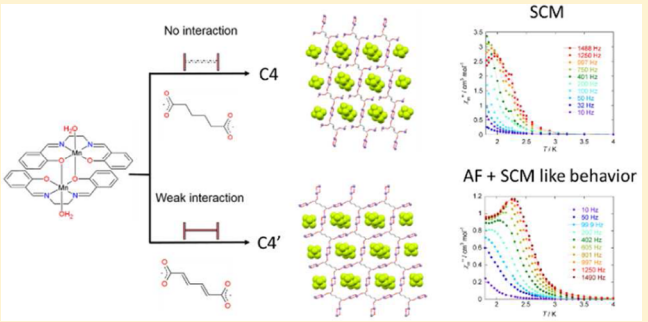

INTRODUCTION

In the field of molecule-based magnets, single-chain magnets (SCMs), described by the Glauber model,[1] have desirable magnetic properties, such as magnetic hysteresis owing to slow relaxation of the magnetization. Since the discovery of the first SCM,[2] their fundamental characteristics and rational design have been investigated by a large number of scientists.[3] Ferromagnetic-like homospin chain $[Mn_2(saltmen)_2Ni(pao)_2(py)_2](ClO_4)_2$ ($saltmen^{2-}$ = *N*,*N*′-(1,1,2,2-tetramethylethyllene)bis(salicylideneimininate), pao^- = pyridine-2-aldoxime, py = pyridine) reported by Clérac, Miyasaka, and co-workers was the first complex exhibiting magnetic dynamics attributed to one-dimensional (1D) correlations in an Ising-like system.[4] In addition, it has been reported that 1D ferrimagnetic cooperative systems beyond the Ising limit ($|D/J| < 4/3$) show SCM dynamics.[5] Collinear spin arrangements have been used to achieve SCM behaviors. In other words, in not only collinear but also noncollinear magnetic chains, SCM-like behaviors have been observed.[6]

In general, in order to develop SCM behavior, interchain interactions must be magnetically suppressed via chemical manipulation, e.g, by employing bulky substituents and/or large counterions. In addition, strong uniaxial anisotropy and 1D-intrachain magnetic correlations, which are described by the Glauber model, are required.[7] On the other hand, incorporation of interchain interactions between SCMs should lead to new magnetic behaviors. In some reported SCM complexes,

Received: May 28, 2015
Published: July 7, 2015

DOI: 10.1021/acs.inorgchem.5b01154
Inorg. Chem. 2015, 54, 7096−7102

interchain interactions have been shown to cause SCM behavior with three-dimensional magnetic ordering.[8] If interchain interactions in SCMs can be controlled by external perturbations, materials switchable between bulk magnets and SCMs could be realized. As mentioned above, understanding the correlation between interchain interaction and SCM behavior is essential for fundamental studies and future applications. In addition, rational synthetic methods to tune the interchain interactions are required to achieve this goal.

In recent years, a few two-dimensional (2D)-network materials containing SCM moieties have been reported.[9] These complexes, in which 1D-magnetic chains are coupled magnetically with weak interactions, exhibit slow relaxation of the magnetization and metamagnetism. Connecting the SCM components with weak interactions between SCMs is a good method for preparing 2D networks. However, rational design of these networks is complicated because three or more moieties are needed to form the network. Moreover, Co^{II} and Fe^{II} ions, which easily oxidize in air, are often used as the metal center. Therefore, less complicated procedures involving fewer building blocks are needed to prepare 2D-network materials composed of SCMs. In addition, rational synthetic methods for preparing SCMs with 2D-network structures could lead to the clarification of the correlation between SCM dynamics and interchain interactions and to progress in the field of switchable SCMs.

Mn^{III} salen-type complexes have been used as the magnetic building block for SCMs because of their negative uniaxial anisotropy (D), stable oxidation states, various derivatives, and substitutable axial sites.[10] At the same time, carboxylic acids can coordinate to two metal ions in a monodentate mode and are often used as bridging ligands because of their various derivatives. In fact, we have reported that 1D chains of Mn^{III} salen-type complexes bridged by carboxylato derivatives show SCM behavior.[11] Therefore, we searched for a simple method to prepare 2D networks of salen-type Mn^{III}-carboxylato 1D-chain complexes linked with dicarboxylato ligands, which can coordinate to four metal ions. Herein, we report the synthesis of 2D-network materials with SCM moieties, where 1D magnetic chains are connected via dicarboxylato linkers with *n*-butyl and butadienyl chains (Scheme 1). In addition, the effects of weak interchain interactions due to the different carbon chains in the linkers on the intrinsic 1D dynamic magnetic properties were investigated.

Scheme 1. Rational Design of 2D-Coordination Polymers

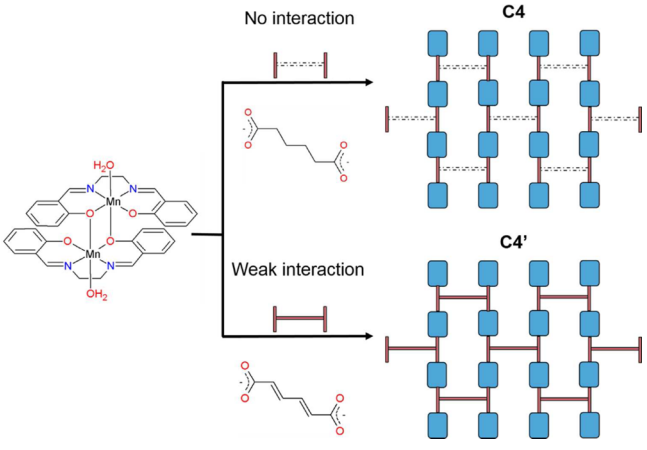

EXPERIMENTAL SECTION

General Procedures and Materials. All reagents and solvents were purchased from Tokyo Kasei Co. Ltd. or Wako Pure Chemical Industries Ltd. and used without further purification. $[Mn(salen)(H_2O)]\cdot(PF_6)$ was prepared according to a previously reported method.[12] All manipulations were performed under aerobic conditions.

Synthesis of $[\{Mn(salen)\}_4(L_1)](PF_6)_2\cdot(CH_3OH)_2$ (**C4**). To a solution of $[Mn(salen)(H_2O)]\cdot(PF_6)$ (193.7 mg, 0.4 mmol) in methanol (10 mL) was added a solution of adipic acid (H_2L1) (14.6 mg, 0.1 mmol) and triethylamine (20.2 mg, 0.2 mmol) in methanol (5 mL). The resulting solution was stirred for 1 h at 60 °C and then filtered. The filtrate was layered with 2-propanol, and over a two-week period, brown plate-type crystals formed. Anal. Calcd (%) for $C_{72}H_{72}N_8F_{12}Mn_4O_{14}P_2$: C, 48.50; H, 4.07; N, 6.28. Found: C, 48.20; H, 4.09; N, 6.47.

Synthesis of $[\{Mn(salen)\}_4(L_2)](PF_6)_2\cdot(CH_3OH)_4$ (**C4′**). To a solution of $[Mn(salen)(H_2O)]\cdot(PF_6)$ (193.7 mg, 0.4 mmol) in methanol (10 mL) was added a solution of *E,E*-1,3-butadiene-1,4-dicarboxylic acid (H_2L2) (14.2 mg, 0.1 mmol) and triethylamine (20.2 mg, 0.2 mmol) in methanol (10 mL). The resulting solution was refluxed for 10 min and then filtered. The filtrate was layered with diethyl ether. After 2 weeks later, brown plate-type crystals were formed. Anal. Calcd (%) for $C_{74}H_{76}N_8F_{12}Mn_4O_{16}P_2$: C, 48.22; H, 4.16; N, 6.08. Found: C, 48.25; H, 3.75; N, 6.41.

Physical Measurements. Magnetic properties were recorded on a Quantum Design SQUID MPMS-XL magnetometer. Direct current (dc) magnetic measurements were performed in the temperature (T) range of 1.8−300 K in the field (H) range of −50−50 kOe. Alternating current (ac) magnetic susceptibilities were obtained in the frequency (f) range 1−1490 Hz with an ac H amplitude of 3 Oe. Ground polycrystalline samples, which were suspended in *n*-eicosane, were placed in a sample holder and mounted in a straw. Experimental data were corrected for the diamagnetic contribution of the sample holder and *n*-eicosane calculated from Pascal constants.

X-ray Crystallography. Single crystals of the complexes coated with Nujol in the mother liquid were mounted on nylon loops and immediately cooled to 108.1 K in a nitrogen cold stream. The data were acquired on a Rigaku CCD diffractometer (Saturn70) with graphite-monochromated Mo Kα radiation (λ = 0.710 70 Å). The crystal dimensions were 0.11 × 0.06 × 0.02 mm^3 for **C4** and 0.17 × 0.15× 0.03 mm^3 for **C4′**. Data were collected and processed using CrystalClear (Rigaku). The linear absorption coefficients, μ, for Mo Kα radiation were 8.006 cm^{-1} for **C4** and 7.656 cm^{-1} for **C4′**. The data were corrected for Lorentz and polarization effects. The structures were solved by using direct methods (SHELXL 97, SIR97, and SIR92). The non-hydrogen atoms were refined anisotropically, and the hydrogen atoms were refined by using a riding model. A Sheldrick weighting scheme was used. All calculations were performed using the Crystal Structure crystallographic software package.

Powder X-ray Diffraction (PXRD) Measurement. PXRD measurements were performed at room T in air on a RIGAKU RINT2500. Since the experimental patterns for **C4** and **C4′** were similar to the patterns simulated from single-crystal X-ray analysis (Supporting Information Figure S2), we concluded that there were no crystalline impurities in **C4** and **C4′**.

RESULTS AND DISCUSSION

Structural Description. From X-ray crystallographic analyses, both **C4** and **C4′** crystallized in the triclinic space group $P\bar{1}$ (Z = 2) with inversion centers at the geometric center of the bridging ligands. X-ray crystallographic data for both **C4** and **C4′** are shown in Table 1. In both cases, the H atoms of the hydroxyl groups of CH_3OH as crystal solvents could not be assigned because of large thermal fluctuation. In one asymmetric unit, as shown in Supporting Information Figure S1, there were two different Mn^{III} ions, which were surrounded by a tetradentate Schiff-base ligand ($salen^{2-}$) and two axial

DOI: 10.1021/acs.inorgchem.5b01154
Inorg. Chem. 2015, 54, 7096−7102

Table 1. Crystallographic Data for C4 and C4′

	C4	C4′
formula	$C_{36}H_{36}N_4F_6Mn_2O_7P$	$C_{37}H_{38}N_4F_6Mn_2O_8P$
fw	891.54	921.57
T/K	108.1	108.1
cryst syst	triclinic	triclinic
space group	$P\bar{1}$ (No. 2)	$P\bar{1}$ (No. 2)
lattice params		
a/Å	12.149(2)	12.012(2)
b/Å	13.216(2)	13. 716(3)
c/Å	14.011(2)	14. 273(2)
α/deg	61.995(8)	63. 277(10)
β/deg	72.171(11)	73. 805(12)
γ/deg	75.034(10)	72. 054(11)
V/Å^3	1873.3(6)	1970.8(6)
Z	2	2
D_{calcd}/g/cm^3	1.580	1.553
F_{000}	910.00	942.00
μ(Mo Kα)/cm^{-1}	8.006	7.656
data measured	15 218	15 833
data unique	8194	8630
R_{int}	0.035	0.027
no. variables	506	524
R1 ($I > 2.00\sigma(I)$)[a]	0.0433	0.0486
wR2 (all reflns)[b]	0.1180	0.1404
GOF	0.988	1.064

[a] $R1 = \sum||F_o| - |F_c||/\sum|F_o|$ ($I > 2.00\sigma(I)$). [b] $wR2 = [\sum w(F_o^2 - F_c^2)^2]/\sum w(F_o^2)^2]^{1/2}$ (all reflns).

oxygen atoms. One axial site was occupied by an out-of-plane phenoxo oxygen atom (O_{ph}) of a neighboring Mn^{III} complex, which led to the formation of dimer unit, [Mn^{III}−(O_{ph})$_2$−Mn^{III}] ([Mn_2]). In general, [Mn_2] type complexes are classified into three types depending on the dimerization distance (Mn^{III}−O_{ph}). Types I, II, and III have shorter Mn^{III}−O_{ph} (~2.5 Å), longer Mn^{III}−O_{ph} (~3.7 Å), and no contact between Mn^{III} ions and O_{ph} atoms, respectively. Thus, both **C4** and **C4′** were classified as type I, meaning that ferromagnetic interactions through the phenoxo bridge ($J_{phenoxo}$) should occur.[13] The other axial site was occupied by a carboxylato oxygen atom (O_{COO}). The two dimer units were connected with *syn*−*anti* carboxylato bridges (−OCO−), which are able to pass antiferromagnetic interactions ($J_{carboxylato}$).[14] As a result, both complexes had 1D-chain structures, {−[$Mn(1)_2$]−OCO−[$Mn(2)_2$]−OCO−[$Mn(1)_2$]−}, in which the nearest-neighbor Mn(1)−Mn(2) distances were determined to be 5.333(1) and 5.490(1) Å for **C4** and **C4′**, respectively. These axial bonds were clearly elongated compared with the equatorial bonds, indicating Jahn−Teller distortion on the Mn^{III} ions (see Supporting Information Table S1). In addition, as shown in Figure 1, the *n*-butyl (−C_4H_8−) and butadienyl chains (−C_4H_4−) in **C4** and **C4′**, respectively, connected the 1D chains into 2D sheets. As shown in Table 2, the shortest interchain Mn−Mn distances were determined to be 8.389 and 9.310 Å in **C4** and **C4′**.

Magnetic Properties. *Direct Current Magnetic Properties.* The T dependences of the magnetic susceptibilities for **C4** and **C4′** were measured on ground polycrystalline samples in the T range from 1.82 to 300 K in an H of 1000 Oe. The plots of the molar magnetic susceptibilities for four Mn^{III} ions multiplied by T, χT, as a function of T are shown in Figure 2. For T > 150 K, the Curie constants (C) and the Weiss

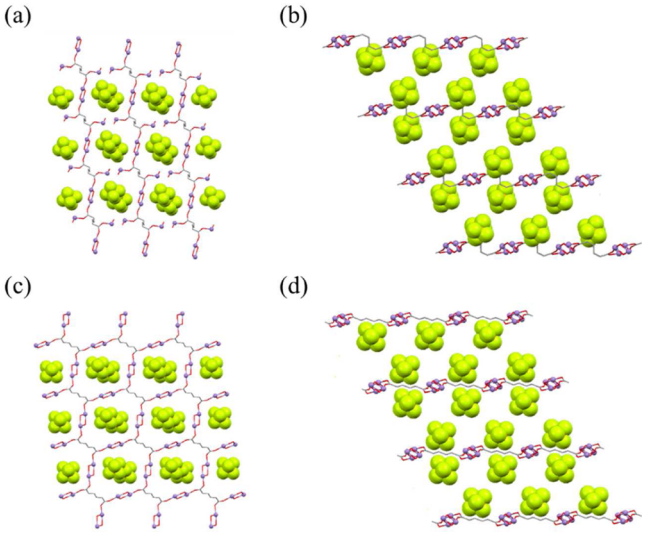

Figure 1. Crystal structure for (a, b) **C4** and (c, d) **C4′**, where counterions (PF_6^-) are represented as CPK models and hydrogen atoms, salen ligands, and solvent molecules were omitted for clarity. Parts a, c and b, d are top and side views of the 2D lattice, respectively.

Table 2. Nearest-Neighbor Interchain Mn−Mn Distances (Å) for C4 and C4′

	C4	C4′
intraplane	Mn(1)−Mn(2)[a]	Mn(1)−Mn(2)[a]
	8.389(1)	9.310
interplane	Mn(1)−Mn(2)[a]	Mn(1)−Mn(2)[a]
	11.811(2)	11.870

[a] Symmetry operations. For **C4**, $-X + 2$, $-Y$, $-Z + 1$. For **C4′**, $-X$, $-Y$, $-Z + 1$.

constants (θ) were estimated to be 12.30 cm^3 K mol^{-1} and 0.6504 K for **C4** and 13.24 cm^3 K mol^{-1} and −3.587 K for **C4′**, respectively, by using the Curie−Weiss law. The calculated C values are close to the spin-only value of 12.00 cm^3 K mol^{-1} for four high-spin Mn^{III} ions. Moreover, the positive value of θ for **C4** indicates that ferromagnetic interactions are dominant, and the negative value for **C4′** indicates that antiferromagnetic interactions are dominant between 150 and 300 K. As shown in Figure 2a, the χT value for **C4** gradually increased with a decrease in T from 12.34 cm^3 K mol^{-1} at 300 K to 13.06 cm^3 K mol^{-1} at 20 K and then decreased to a minimum of 12.27 cm^3 K mol^{-1} at 5.8 K. This behavior is due to $J_{phenoxo}$ in the T range 20−300 K, where the χT values increased, and $J_{carboxylato}$ when T < 20 K, where the χT values decreased.[13,14] The sharp increase in the χT value with a decrease in T is due to weak ferromagnetic behavior from spin canting, arising from zigzag-shaped chain structure of **C4**. In the case of **C4′**, as shown in Figure 2b, with a decrease in T, the χT value became a minimum of 10.54 cm^3 K mol^{-1} at 5.0 K due to $J_{carboxylato}$. Then, the χT value abruptly increased to 11.07 cm^3 K mol^{-1} at 2.8 K with a further decrease in T. This implies that $J_{phenoxo}$ is active in **C4′**. The results of the magnetic measurements indicate that a 1D-spin system, {−[Mn(1)−$J_{phenoxo}$−Mn(1)]−$J_{carboxylato}$−[Mn(2)−$J_{phenoxo}$−Mn(2)]−$J_{carboxylato}$−}, is formed in both **C4** and **C4′**. In order to compare the magnetic behavior for **C4** and that for **C4′**, the semiquantitative analysis of the exchange parameters for both **C4** and **C4′** were performed between 10

DOI: 10.1021/acs.inorgchem.5b01154
Inorg. Chem. 2015, 54, 7096−7102

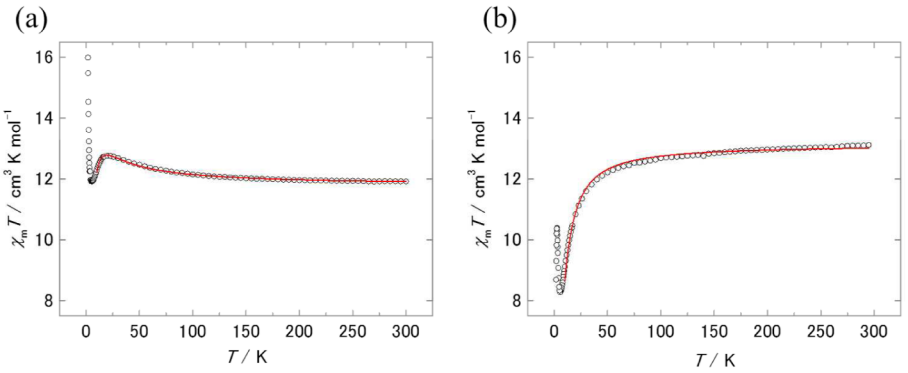

Figure 2. T dependence of χT in an H of 1000 Oe for (a) **C4** and (b) **C4′**. Circles and solid lines represent experimental data and curve fittings, respectively.

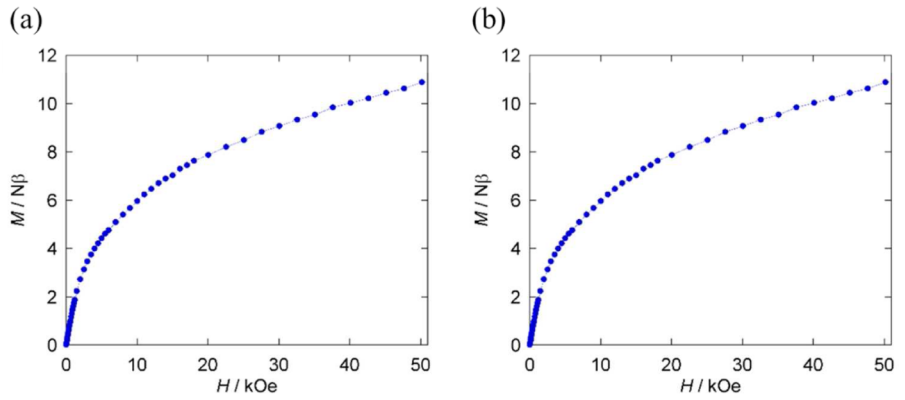

Figure 3. Magnetization for (a) **C4** and (b) **C4′** as a function of the applied H at 1.82 K. Solid lines are guides for eyes.

and 300 K by using $S = 2$ spin dimer model with mean-field approximation.[14]

$$\chi_M = \frac{\chi_m}{1 - (2zJ'/Ng^2\mu_B{}^2)\chi_m} \quad (1)$$

where

$$\chi_m = \frac{Ng^2\mu_B{}^2}{k_BT}\frac{2\exp(2x) + 10\exp(6x) + 28\exp(12x) + 60\exp(20x)}{1 + 3\exp(2x) + 5\exp(6x) + 7\exp(12x) + 9\exp(20x)}$$

$$x = 2J/k_BT$$

In eq 1, J was defined as an intradimer [Mn^{III}−(O$_{ph}$)$_2$−Mn^{III}] ferromagnetic-exchange coupling. On the other hand, zJ' included antiferromagnetic interactions with carboxylato bridging [Mn$_2$]−OCO−[Mn$_2$] ($J_{carboxylato}$) and intra- and interplane dipole−dipole interactions for both **C4** and **C4′**. Such an approximation is necessary since there are too many parameters to perform a complete analysis. This simple model can be used to evaluate the dominant magnetic interaction for **C4** and **C4′**. Least-squares curve fittings of the magnetic susceptibility data by eq 1 converged with $J = 0.54$ cm^{-1}, $zJ' = -0.12$ cm^{-1}, $g = 1.98$ for **C4**, and $J = 0.47$ cm^{-1}, $zJ' = -0.35$ cm^{-1}, $g = 2.08$ for **C4′**, respectively (see Figure 2). Focusing on antiferromagnetic interactions, the zJ' value for **C4′** is larger than that for **C4**. This indicates that zJ' for **C4** is intrinsically caused by only antiferromagnetic interactions due to $J_{carboxylato}$ while **C4′** possesses not only $J_{carboxylato}$ but also J_{linker} through the π-conjugated butadienyl linkers from the viewpoints of crystal structure for both compounds.

Figure 3 shows magnetization curves for **C4** and **C4′** at 1.82 K. Up to $H = 50$ kOe, the magnetizations of both complexes did not saturate up to 16.00 $N\mu_B$, which is consistent with the magnetization value expected for four high-spin Mn^{III} ions. The results indicated that there were antiferromagnetic interactions or magnetic anisotropy due to Jahn−Teller distortion of the high-spin Mn^{III} ions. As shown in Figure 3a, the magnetization of **C4** monotonically increased up to $H = 50$ kOe. On the other hand, the magnetization of **C4′** shown in Figure 4 developed as a sigmoidal magnetization curve in the lower H region (≤5 kOe), which indicated spin-flip due to antiferromagnetic interactions. Moreover, in the first differential curve of the magnetization, a peak appeared at 800 Oe, from which the

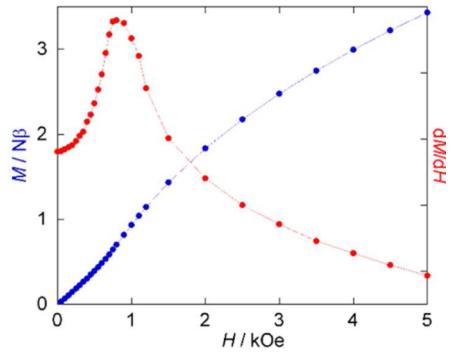

Figure 4. Magnetization (blue) and first H derivative of magnetization (red) as a function of the applied H for **C4′** at 1.82 K. Solid lines are guides for eyes.

DOI: 10.1021/acs.inorgchem.5b01154
Inorg. Chem. 2015, 54, 7096−7102

antiferromagnetic interactions were estimated to be 0.027 K by using $2|zJ'|S^2 = gS\mu_B H_{ex}$. This value is much smaller than that of the carboxylato bridge ($J_{carboxylato}$ = 0.1−1.0 K).[14] Therefore, we attributed the peak at 800 Oe to weak antiferromagnetic interchain interactions through J_{linker}.[9g] Furthermore, the magnetization curve for **C4′** depended on T, and the peak in the first differential curve of the magnetization disappeared above 2.3 K, as shown in Figure 5 indicating the suppression of

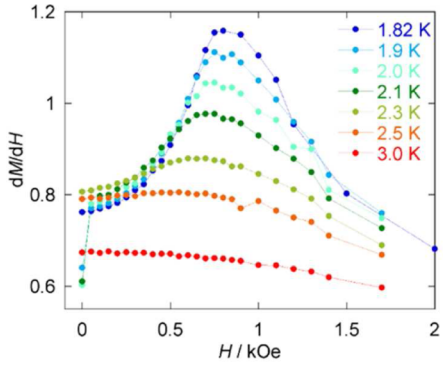

Figure 5. First H derivatives of the magnetization as a function of the applied H for **C4′** below 3.0 K. Solid lines are guides for eyes.

J_{linker} by heating. In order to confirm an antiferromagnetic phase transition, the static magnetic measurements were performed in an H of 50 Oe for **C4′** (see Supporting Information Figure S5). The Néel temperature point was observed at 2.3 K. Thus, **C4′** behaves as an antiferromagnet when T < 2.3 K and H < 800 Oe.

Alternating Current Magnetic Properties. The in-phase (χ') and out-of-phase (χ'') ac magnetic susceptibilities for **C4** and **C4′** as a function of T in the f range 10−1490 Hz in a zero H are shown in Figure 6. Both χ' and χ'' were clearly dependent on the frequencies, which indicated slow relaxation of the magnetization. It is noteworthy that ac magnetic susceptibilities for **C4′** depend on the frequencies around the Néel temperature. The activation energy (Δ_τ/k_B) and the frequency factor of the relaxation time (τ_0) were estimated from the peak tops of χ'' in Figure 6b for **C4** and in Figure 6d for **C4′** by using the Arrhenius law:

$$\tau = \tau_0 \exp\left(\frac{\Delta_\tau}{k_B T}\right) \quad (2)$$

From eq 2, Δ_τ/k_B and τ_0 were 18.65 K and 8.86×10^{-9} s for **C4** and 22.41 K and 6.39×10^{-9} s for **C4′**, respectively. In addition, the origins of dynamic properties of **C4** and **C4′** were examined in relation to the Mydosh parameter, $\phi = \Delta T_\nu/(T_\nu \Delta \log f)$. The values were estimated to be 0.23 for **C4** and 0.25 for **C4′**. In general, the ϕ value for superparamagnets is larger than 0.1.[15] Thus, slow relaxation of the magnetization in both **C4** and **C4′** is due to superparamagnetism rather than a spin glass behavior. As shown in Figure 6b, χ'' for **C4** exhibited only one peak in the T range 1.82−4.0 K at each frequency. On the other hand, χ'' for **C4′** exhibited a peak in the T range 2.0−2.5 K, and anomalous features were observed when below the Néel temperature (2.3 K) at f > 400 Hz, as shown in Figure 6d. The low-T features have been observed for 1D ferrimagnetic chains exhibiting slow relaxation of the magnetization with a broad τ distribution due to interchain interactions.[9g,16] Thus, the χ'' anomaly for **C4′** was attributed to the antiferromagnetic phase transition derived from weak J_{linker}. In order to confirm the influence of J_{linker} on the dynamics for **C4′**, ac magnetic measurements in the field 1000 Oe which could suppress J_{linker} were performed in the temperature range 1.82−3.0 K. Figure 7 shows the ac susceptibilities as a function of temperature for **C4′** in 1000 Oe at various frequencies. The values of Δ_τ/k_B, τ_0, and ϕ are estimated to be 28.13 K, 1.940×10^{-10} s, and 0.16, respectively. It is interesting to note that ac susceptibilities are obviously different with/without field and that the shoulders

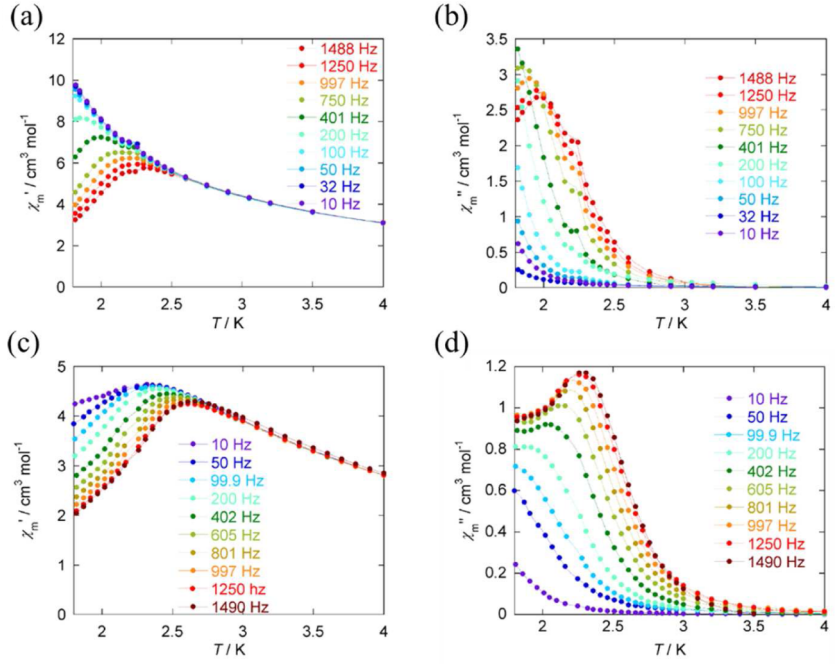

Figure 6. T dependence of (a, c) in-phase (χ') and (b, d) out-of-phase (χ'') ac susceptibilities for **C4** and **C4′**, respectively, in the f range 10−1490 Hz in a zero H. Solid lines are guides for eyes.

DOI: 10.1021/acs.inorgchem.5b01154
Inorg. Chem. 2015, 54, 7096−7102

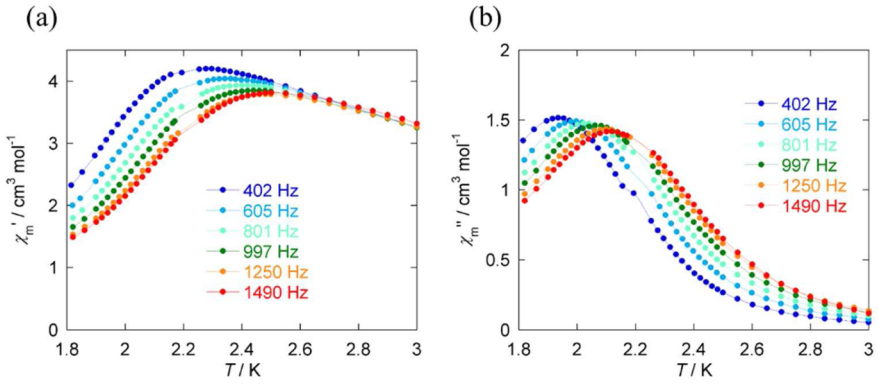

Figure 7. T dependence of (a) in-phase (χ') and (b) out-of-phase (χ'') ac susceptibilities for **C4′**, respectively, in the f range 10−1490 Hz in an H of 1000 Oe. Solid lines are guides for eyes.

below 2 K in Figure 5d disappear. This is the evidence that magnetic relaxation for **C4′** is affected by J_{linker} and that the width of relaxation time due to antiferromagnetic coupling between chains can be converged by applying field (≥1000 Oe).

The $\ln(\chi'T)$ was plotted against T^{-1}, as shown in Supporting Information Figure S7 to confirm the occurrence of the magnetic correlations in **C4** and **C4′**. The $\ln(\chi'T)$ increased linearly with an increase in T^{-1} in the T range of 2.6−3.5 K for **C4** and 3.2−4.5 K for **C4′**. The correlation energies, Δ_ξ/k_B, were estimated to be 0.99 K for **C4** and 0.59 K for **C4′** by using eq 3.

$$\chi'T = C_{eff} \exp\left(\frac{\Delta_\xi}{k_B T}\right) \tag{3}$$

Thus, we concluded that **C4** and **C4′** exhibited 1D-magnetic correlation and SCM-like behavior. However, it is known that the Δ_ξ values for the SCMs with antiferromagnetic nonlinear spin arrangements determined by using eq 2 are lower than the true values.[6] Therefore, the true Δ_ξ values for **C4** and **C4′** could be larger than the experimental values.

χ values were determined as a function of f in the T range 1.82−2.1 K for **C4** and 1.82−2.4 K for **C4′** in a zero H (Supporting Information Figures S8 and S9, respectively). These results were fitted by using a generalized Debye model

$$\chi'(\omega) = \chi_S + (\chi_T + \chi_S)\frac{1 + (\omega\tau)^{1-\alpha}\sin\left(\frac{\pi\alpha}{2}\right)}{1 + 2(\omega\tau)^{1-\alpha}\sin\left(\frac{\pi\alpha}{2}\right) + (\omega\tau)^{2-2\alpha}} \tag{4a}$$

$$\chi''(\omega) = (\chi_T + \chi_S)\frac{(\omega\tau)^{1-\alpha}\cos\left(\frac{\pi\alpha}{2}\right)}{1 + 2(\omega\tau)^{1-\alpha}\sin\left(\frac{\pi\alpha}{2}\right) + (\omega\tau)^{2-2\alpha}} \tag{4b}$$

where α is the dispersion coefficient of the relaxation of magnetization. When α approaches zero, the magnetic relaxation process is an ideal single process. The values of τ_0, Δ_τ, and α are summarized in Table 3. The α value is smaller than 0.1, which means that the relaxation process is close to an ideal single relaxation process and that there is no magnetic perturbation toward the SCM behavior for **C4**. The α value at 1.82 K for **C4′** was determined to be 0.33, which is greater than that for **C4**. The SCM-like behavior for **C4′** does not involve a single relaxation process. In general, α indicates the distribution width of τ. Thus, the broad distribution of τ for **C4′** was attributed to J_{linker}. In the T dependence of α for **C4** and **C4′** shown in Figure 8, a correlation was clearly observed, which is consistent with the increasing effects of J_{linker} with a decrease in T. In the case of **C4**, a linear increase in α with an increase in T^{-1} was observed. In contrast, for **C4′**, there were two linear regions for α, and they crossed at 2.2 K. This intersection T corresponds to the Néel temperature being suppressed, and thus, the abrupt increase in α below 2.2 K is due to J_{linker}. Thus, the effects of antiferromagnetic coupling between SCM-like behaviors, which broaden the τ distribution, were directly observed via α versus T^{-1} plots. Furthermore, in ln τ versus T^{-1} plots, there was an inflection point at the Néel temperature, indicating that J_{linker} had also an effect on the relaxation times (see Supporting Information Figure S9). In a field of 1000 Oe, α for **C4′** linearly increased with an increase in T^{-1} (see Supporting Information Figure S11). In other words, in an applying field, α for **C4′** behaved in the same way as that for **C4** without antiferromagnetic coupling between 1D-chains.

Table 3. Parameters Obtained by Fitting χ'' for C4 and C4′ in a Zero H with Generalized Debye Model

	C4	C4′
τ_0/s	1.989×10^{-8}	$1.956 \times 10^{-8}/8.142 \times 10^{-7}$
Δ_τ/k_B/K	17.88	19.08/11.29
α	≤0.095 91	≤0.334 13

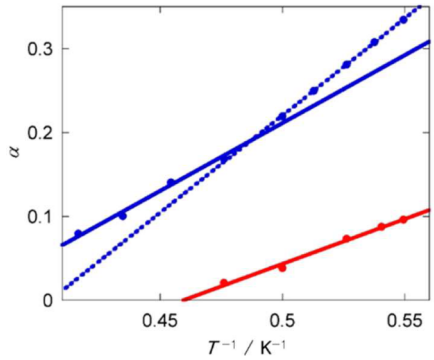

Figure 8. Dispersion coefficient (α) as a function of T^{-1} for **C4** (red) and **C4′** (blue). Lines represent linear fits obtained by using least-squares method.

DOI: 10.1021/acs.inorgchem.5b01154
Inorg. Chem. 2015, 54, 7096−7102

SUMMARY

In this study, we presented a simple method for preparing 2D-network materials containing SCM moieties by using a one-pot reaction involving a Mn^{III} Schiff-base complex and dicarboxylic acids. In the static magnetic measurements for **C4′**, an antiferromagnetic phase transition was observed. From ac magnetic measurements, both **C4** and **C4′** showed slow relaxation of the magnetization due to intrinsic 1D magnetic correlations. **C4** exhibited SCM behavior with a single relaxation process. On the other hand, for **C4′**, the ac susceptibility depended on the frequencies around the Néel temperature. Moreover, α versus T^{-1} plots for **C4′** had an inflection point, which was attributed to weak antiferromagnetic interactions through the π-conjugated orbital pathway of the butadienyl chain of the linkers. In other words, by changing the linker from a saturated to an unsaturated aliphatic group, weak interactions were incorporated between the SCM moieties. Furthermore, we realized that the antiferromagnetic coupling due to J_{linker} directly had an effect on the distribution width of τ for **C4′**. The results of this study will make it possible to design and prepare new magnetically coupled 2D nanomaterials

ASSOCIATED CONTENT

Supporting Information

Additional crystallographic and magnetization data. Crystallographic data in CIF format. The Supporting Information is available free of charge on the ACS Publications website at DOI: 10.1021/acs.inorgchem.5b01154.

AUTHOR INFORMATION

Corresponding Authors

*E-mail: kagesawa@m.tohoku.ac.jp.

*E-mail: yamasita@agnus.chem.tohoku.ac.jp.

Notes

The authors declare no competing financial interest.

REFERENCES

(1) Glauber, R. J. *J. Math. Phys.* **1963**, *4*, 294.

(2) Caneschi, A.; Gatteschi, D.; Lalioti, N.; Sessoli, R.; Venturi, G.; Vindigni, A.; Rettori, A.; Pini, M. G.; Novak, M. A. *Angew. Chem., Int. Ed.* **2001**, *40*, 1760.

(3) (a) Miyasaka, H.; Madanbashi, T.; Sugimono, K.; Nakazawa, Y.; Wernsdorfer, W.; Sugiura, K.; Yamashita, M.; Clérac, R. *Chem. - Eur. J.* **2006**, *12*, 7028. (b) Coulon, C.; Clérac, R.; Lecren, L.; Wernsdorfer, W.; Miyasaka, H. *Phys. Rev. B: Condens. Matter Mater. Phys.* **2004**, *69*, 132408. (c) Liu, T.; Zheng, H.; Kang, S.; Shiota, Y.; Hayami, S.; Mito, M.; Sato, O.; Yoshizawa, K.; Kanezawa, S.; Duan, C. *Nat. Commun.* **2013**, *4*, 2826. (d) Ding, M.; Wang, B.; Wang, Z.; Zhang, J.; Fuhr, O.; Fenske, D.; Gao, S. *Chem. - Eur. J.* **2012**, *18*, 915. (e) Bernot, K.; Bogani, L.; Caneschi, A.; Gatteschi, D.; Sessoli, R. *J. Am. Chem. Soc.* **2006**, *128*, 7947.

(4) Clérac, R.; Miyasaka, H.; Yamashita, M.; Coulon, C. *J. Am. Chem. Soc.* **2002**, *124*, 12837.

(5) Zhang, W.-X.; Ishikawa, R.; Breedlove, B. K.; Yamashita, M. *RSC Adv.* **2013**, *3*, 3772.

(6) Bernot, K.; Luzon, J.; Sessoli, R.; Vindigni, A.; Thion, J.; Richeter, S.; Leclercq, D.; Larionova, J.; van der Lee, A. *J. Am. Chem. Soc.* **2008**, *130*, 1619.

(7) Miyasaka, H.; Clérac, R. *Bull. Chem. Soc. Jpn.* **2005**, *78*, 1725.

(8) (a) Miyasaka, H.; Takayama, K.; Saitoh, A.; Furukawa, S.; Yamashita, M.; Clérac, R. *Chem. - Eur. J.* **2010**, *16*, 3656. (b) Coulon, C.; Clérac, R.; Wernsdorfer, W.; Colin, T.; Miyasaka, H. *Phys. Rev. Lett.* **2009**, *102*, 167204.

(9) (a) Zheng, Y.-Z.; Tong, M.-L.; Zhang, W.-X.; Chen, X.-M. *Angew. Chem., Int. Ed.* **2006**, *45*, 6310. (b) Zhang, X.-M.; Wang, Y.-Q.; Wang, K.; Gao, E.-Q.; Liu, C.-M. *Chem. Commun.* **2011**, *47*, 1815. (c) Wang, Y.-Q.; Zhang, X.-M.; Li, X.-B.; Wang, B.-W.; Gao, E.-Q. *Inorg. Chem.* **2011**, *50*, 6314. (d) Wang, Y.-Q.; Sun, W.-W.; Wang, Z.-D.; Jia, Q.-X; Gao, E.-Q.; Song, Y. *Chem. Commun.* **2011**, *47*, 6386. (e) Wöhlert, S.; Ruschewitz, U.; Näther, C. *Cryst. Growth Des.* **2012**, *12*, 2715. (f) Wöhlert, S.; Boeckmann, J.; Wriedt, M.; Näther, C. *Angew. Chem., Int. Ed.* **2011**, *50*, 6920. (g) Toma, L. M.; Ruiz-Pérez, C.; Pasán, J.; Wernsdorfer, W.; Lloret, F.; Julve, M. *J. Am. Chem. Soc.* **2012**, *134*, 15265.

(10) (a) Kennedy, B. J.; Murray, K. *Inorg. Chem.* **1985**, *24*, 1552. (b) Lü, Z.-L.; Yuan, M.; Pan, F.; Gao, S.; Zhang, D.-Q.; Zhu, D.-B. *Inorg. Chem.* **2006**, *45*, 3538. (c) Miyasaka, H.; Clérac, R.; Wernsdorfer, W.; Lecren, L.; Bonhomme, C.; Sugiura, K.; Yamashita, M. *Angew. Chem., Int. Ed.* **2004**, *43*, 2801.

(11) Zhang, W.-X.; Shiga, T.; Miyasaka, H.; Yamashita, M. *J. Am. Chem. Soc.* **2012**, *134*, 6908.

(12) Miyasaka, H.; Nezu, T.; Sugimoto, K.; Sugiura, K.; Yamashita, M.; Clérac, R. *Chem. - Eur. J.* **2005**, *11*, 1592.

(13) Miyasaka, H.; Clérac, R.; Ishii, T.; Chang, H.-C.; Kitagawa, S.; Yamashita, M. *J. Chem. Soc., Dalton Trans.* **2002**, 1528.

(14) (a) Huang, D.; Wang, W.; Zhang, X.; Chen, C.; Chen, F.; Liu, Q.; Liao, D.; Li, Licun; Sun, L. *Eur. J. Inorg. Chem.* **2004**, *2004*, 1454. (b) Rodriguez-Martin, Y.; Hernandez-Molina, M.; Sanchiz, J.; Ruiz-Pérez, C.; Lloret, F.; Julve, M. *Dalton Trans.* **2003**, 2359. (c) Durot, S.; Policar, C.; Pelosi, G.; Bisceglie, F.; Mallah, T.; Mahy, J.-P. *Inorg. Chem.* **2003**, *42*, 8072. (d) Gómez, V.; Corbella, M. *Eur. J. Inorg. Chem.* **2009**, *2009*, 4471. (e) Mitra, K.; Mishra, D.; Biswas, S.; Lucas, R.; Adhikary, B. *Polyhedron* **2006**, *25*, 1681.

(15) Mydosh, J. A. *Spin Glasses: An Experimental Introduction*; Taylor & Francis: London, 1993.

(16) Ferrando-Soria, J.; Pardo, E.; Ruiz-García, R.; Cano, J.; Lloret, F.; Julve, M.; Journaux, Y.; Pasán, J.; Ruiz-Pérez, C. *Chem. - Eur. J.* **2011**, *17*, 2176.

DOI: 10.1021/acs.inorgchem.5b01154
Inorg. Chem. 2015, 54, 7096−7102